

AAV-mediated gene therapy for galactosialidosis: A long-term safety and efficacy study

Huimin Hu,¹ Rosario Mosca,¹ Elida Gomero,¹ Diantha van de Vlekkert,¹ Yvan Campos,¹ Leigh E. Fremuth,^{1,2} Scott A. Brown,³ Jason A. Weesner,^{1,2} Ida Annunziata,¹ and Alessandra d'Azzo^{1,2}

¹Department of Genetics, St. Jude Children's Research Hospital, Memphis, TN, USA; ²Department of Anatomy and Neurobiology, College of Graduate Health Sciences, University of Tennessee Health Science Center, Memphis, TN 38163, USA; ³Department of Immunology, St. Jude Children's Research Hospital, 262 Danny Thomas Place, Memphis, TN 38105, USA

AAV-mediated gene therapy holds promise for the treatment of lysosomal storage diseases (LSDs), some of which are already in clinical trials. Yet, ultra-rare subtypes of LSDs, such as some glycoproteinoses, have lagged. Here, we report on a long-term safety and efficacy preclinical study conducted in the murine model of galactosialidosis, a glycoproteinosis caused by a deficiency of protective protein/cathepsin A (PPCA). One-month-old *Ctsa*^{-/-} mice were injected intravenously with a high dose of a self-complementary AAV2/8 vector expressing human *CTSA* in the liver. Treated mice, examined up to 12 months post injection, appeared grossly indistinguishable from their wild-type littermates. Sustained expression of scAAV2/8-*CTSA* in the liver resulted in the release of the therapeutic precursor protein in circulation and its widespread uptake by cells in visceral organs and the brain. Increased cathepsin A activity resolved lysosomal vacuolation throughout the affected organs and sialyl-oligosacchariduria. No signs of hyperplasia or inflammation were detected in the liver up to a year of age. Clinical chemistry panels, blood cell counts, and T cell immune responses were normal in all treated animals. These results warrant a close consideration of this gene therapy approach for the treatment of galactosialidosis, an orphan disease with no cure in sight.

INTRODUCTION

Galactosialidosis (GS) is a glycoprotein storage disease caused by mutations in the *CTSA* gene, encoding the lysosomal carboxypeptidase protective protein/cathepsin A (PPCA). PPCA assembles into a lysosomal multienzyme complex (LMC) with the glycosidases β -galactosidase (β -GAL) and neuraminidase 1 (NEU1), a configuration that renders these enzymes catalytically active and stable in lysosomes.¹ A congenital defect of PPCA alters complex formation, leading to loss of NEU1 activity and reduced (~15%–20%) β -GAL activity.^{2,3} To date, the combined deficiency of the three enzymes in the complex remains the biochemical and diagnostic hallmark of GS. The severe secondary deficiency of NEU1 accounts for the presence of sialylated glycoproteins and oligosaccharides in tissues and body fluids, a feature that GS shares with sialidosis, caused by the isolated deficiency of NEU1.⁴

Based on the age of onset and severity of their clinical symptoms, GS patients are classified into three subtypes: early infantile, late infantile, and juvenile/adult. The severe early infantile forms of the disease present with a systemic condition associated with fetal hydrops, skeletal dysplasia, visceromegaly, renal and cardiac failure, neurological involvement, and premature death.² The late infantile forms comprise a distinct group of patients with mild or absent cognitive involvement. In this group, clinical manifestations appear in the first decade of life and continue into adulthood. They include coarse facies, dysostosis multiplex, growth retardation, heart and kidney problems, and hearing loss.² About 60% of GS clinical cases belong to the juvenile/adult group, mainly of Japanese descent.² Although these patients can have a normal life expectancy, they develop severe clinical signs, including myoclonus, ataxia, neurological symptoms, mental retardation, and angiokeratoma without visceral involvement. The early-onset patients are genetically the most heterogeneous, while the late infantile and juvenile/adult patients may share allelic variants that segregate with these clinical phenotypes.

The only mouse model of GS (*Ctsa*^{-/-}, formerly referred to as *PPCA*^{-/-}) currently available was generated by disruption of the *Ctsa* gene, as previously described.⁵ *Ctsa*^{-/-} mice have a reduced lifespan (~7 months) and already display signs of the disease at birth, being visibly smaller than their wild-type (WT) or heterozygous littermates.⁵ The early onset and severity of their systemic and neurological phenotypes parallel the clinical manifestations described in GS patients of the early infantile group. At the mid-end stage of the disease, *Ctsa*^{-/-} mice develop diffuse edema associated with inflammation of the eyelids and

Received 19 July 2021; accepted 26 October 2021;
<https://doi.org/10.1016/j.omtm.2021.10.007>.

Correspondence: Ida Annunziata, PhD, Department of Genetics, St. Jude Children's Research Hospital, Memphis, TN, USA.

E-mail: ida.annunziata@stjude.org

Correspondence: Alessandra d'Azzo, PhD, Department of Genetics, St. Jude Children's Research Hospital, Memphis, TN, USA. Department of Anatomy and Neurobiology, College of Graduate Health Sciences, University of Tennessee Health Science Center, Memphis, TN 38163, USA.

E-mail: sandra.dazzo@stjude.org

thickening of the paws. The occurrence of neurological symptoms, such as tremor, ataxia, and abnormal gait, coincides with progressive loss of Purkinje cells in the cerebellum.^{5,6} Histopathological examination of *Ctsa*^{-/-} mice during the preweaning period has revealed widespread lysosomal expansion and storage in cells of the most affected organs, such as kidney, small intestine, liver, and choroid plexus. Overall, cells of the reticuloendothelial or macrophage system are also the primary target of the disease in the mouse model.⁵ The severe renal involvement, a prominent sign of GS in patients, is fully recapitulated in the *Ctsa*^{-/-} mice and results in progressive sialyl-oligosacchariduria. Primary deficiency of cathepsin A (CA) is accompanied by the total loss of NEU1 activity, while β -Gal activity is reduced in certain cells, such as skin fibroblasts, in only the early stages of the disease, but gradually increases in most organs as the disease progresses.⁵

Target therapy for GS is still investigational, but several treatment options, which hold promise for the treatment of patients, have been tested in the *Ctsa*^{-/-} mice, ranging from bone marrow (BM)-mediated *ex vivo* gene therapy to enzyme replacement therapy (ERT) and adeno-associated virus (AAV)-mediated *in vivo* gene therapy.^{5,7-9} In recent years, AAV has emerged as the preferred *in vivo* gene transfer system for the treatment of lysosomal storage diseases (LSDs) because of its efficacy of infection, broad tropism, and safety. Multiple AAV serotypes have been engineered with increased tropism for specific cell populations (e.g., hepatocytes and neurons) and have been tested in LSD patients and animal models.^{10,11} We have experimented with a self-complementary AAV2/8 vector (scAAV2/8-LP1-*hCTSA*, hereafter scAAV2/8-CTSA) with restricted expression of a human CTSA transgene to the liver, driven by a liver-specific enhancer-promoter combination.⁷ In a dose-finding, preclinical study, *Ctsa*^{-/-} mice were treated at 1 month of age with three escalating doses of the recombinant vector, resulting in a clear reversal of several clinical signs, including edema, gait defects, and oligosacchariduria.

Given the positive outcome of this therapeutic approach, we have now designed a comprehensive study performed in *Ctsa*^{-/-} mice treated with a high dose (2×10^{13} gc/kg) of scAAV2/8-CTSA, with the intent to evaluate AAV biodistribution; long-term efficacy and safety, including the potential occurrence of inflammation and neoplasia; and the presence of neutralizing antibodies. In addition to the correction of histopathological, biochemical, and clinical phenotypes, we demonstrate that the systemic administration of a high dose of the recombinant vector did not elicit any adverse effect, including liver toxicity, immune response, and hyperplasia. To our knowledge, this is one of the few studies aimed at characterizing potential toxicity associated with AAV-mediated gene therapy, which will facilitate the development of a safe and effective therapy for this orphan LSD.

RESULTS

Biodistribution of recombinant AAV in tissues of treated *Ctsa*^{-/-} mice

To test the long-term effects of administering a single high dose of recombinant vector, a cohort of *Ctsa*^{-/-} mice were treated with scAAV2/8-CTSA at a concentration of 2×10^{13} vg/kg, two times

Table 1. Study design for mice receiving scAAV2/8LP1-hPPCA or vehicle treatment

Group	Test article(s)	Gender ^a	Genotype	Terminal collection time point
1 (Control)	vehicle	M/F	WT	7 days–12 months
2 (Control)	vehicle	M/F	<i>Ctsa</i> ^{-/-}	7 days–7 months
3	scAAV2/8LP1-CTSA	M/F	<i>Ctsa</i> ^{-/-}	7 days
4	scAAV2/8LP1-CTSA	M/F	<i>Ctsa</i> ^{-/-}	1 month
5	scAAV2/8LP1-CTSA	M/F	<i>Ctsa</i> ^{-/-}	3 months
6	scAAV2/8LP1-CTSA	M/F	<i>Ctsa</i> ^{-/-}	6 months
7	scAAV2/8LP1-CTSA	M/F	<i>Ctsa</i> ^{-/-}	12 months

^an = 4 mice per group, 2 males and 2 females.

higher than the highest vector dose used previously (1×10^{11} vg/kg).⁷ Male and female mice were randomized and grouped into seven cohorts (Table 1) with a group size of four scAAV2/8-CTSA-injected (two males and two females) mice and an equal number of WT and *Ctsa*^{-/-} vehicle-injected controls (Table 1). *Ctsa*^{-/-} mice were injected intravenously at 1 month of age and analyzed at 7 days and 1, 3, 6, and 12 months post injection. All injected *Ctsa*^{-/-} mice survived the treatment and outlived the knockout (KO) mice that died, on average, at \sim 7 months of age. Therefore, the eldest KO mice used as controls for evaluating efficacy of this therapeutic approach were \sim 7 months of age.

We first assessed the vector biodistribution by measuring the copy number of recombinant scAAV2/8-CTSA in the total genomic DNA extracted from multiple organs of treated mice at 12 months post injection. As expected, the highest viral load (average of 1.04×10^6) was detected in the liver, the intended target organ, followed by lymph nodes, diaphragm, heart, ovary, and lung (Figure 1A). The other tissues had 2 log₂ lower amounts of viral genome compared to the liver, with the pancreas containing the lowest copy number (average of 7.76×10^2) (Figure 1A). Low but still detectable levels of viral genome were measured in the brain of treated mice (average of 1.03×10^4). Comparing AAV levels in the liver with those in the brain, we noticed a similar pattern of a gradual decrease in measurable viral genome from 7 days (4.09×10^6 in the liver and 2.79×10^4 in the brain) to 1 year (1.04×10^6 in the liver and 1.03×10^4 in the brain) post injection (Figures 1B and 1C).

High CA activity in AAV-treated *Ctsa*^{-/-} mice restores the function of the LMC

Ctsa^{-/-} mice treated with scAAV2/8-CTSA showed clear improvement of their gross phenotype and were nearly indistinguishable from their WT counterparts at all time points, including at 12 months post injection; their food intake was normal, and their generalized edema and infertility were entirely resolved. No consistent gender differences were recorded between male and female mice in their response to treatment, but rather, there was variability among animals. Therefore, the data for both gender groups were combined.

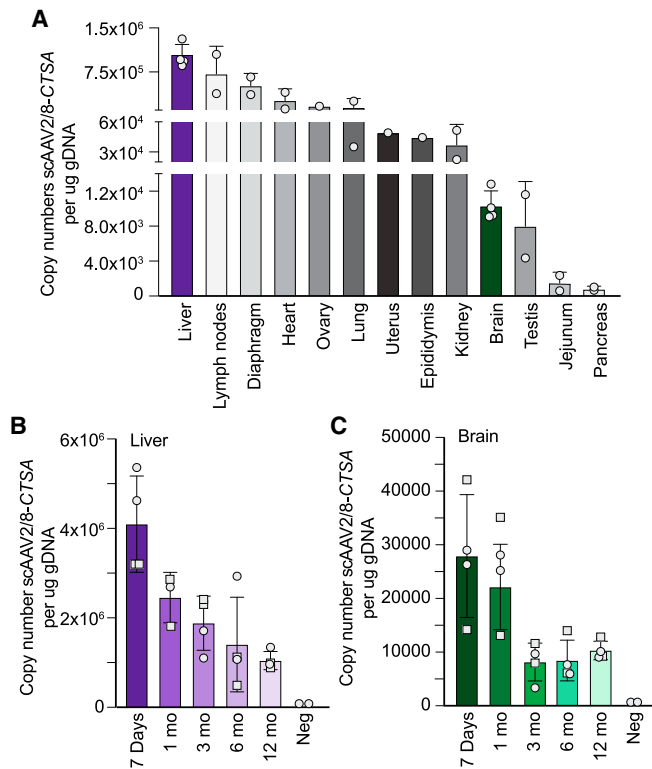


Figure 1. Biodistribution of recombinant AAV in *Ctsa*^{-/-} mice

(A) scAAV2/8-CTSA copy number in multiple organs of injected animals isolated 12 months post injection, measured per milligram of genomic DNA. (B, C) scAAV2/8-CTSA copy number shown in the (B) liver and (C) brain collected at day 7, and at 1, 3, 6, and 12 months following AAV-mediated gene transfer. Round symbols depict males, while square symbols depict females ($n \geq 2$).

The efficacy of infection was first determined by measuring the expression levels of therapeutic PPCA in key target tissues of AAV-injected mice at all time points. Predictably, maximum CA activity was measured in the liver, where enzyme levels reached values ~250 times higher than those of WT mice at 7-day (200 times) and 1-month (300 times) time points and remained ~85 times higher than controls at 12 months post injection (Figures 2A and S1A). The sustained and persistent expression of the therapeutic enzyme in the liver resulted in the release of the PPCA zymogen into the circulation, as demonstrated by the correction of both CA and NEU1 activities in GS patients' fibroblasts after the addition of serum samples from AAV-treated mice to the culture medium (Figure S2). The circulating precursor was efficiently recaptured by deficient cells in visceral organs and in the brain. Spleen and kidney were chosen as representative organs because of their opposing response to therapeutic PPCA (Figures 2B, 2C, S1B, and S1C). Being a hematopoietic organ, splenocytes readily captured the therapeutic enzyme, as demonstrated by the dramatic increase in CA activity measured in this organ throughout the duration of the treatment (Figures 2B and S1B). On the opposite side, the kidney, a less accessible organ and one mainly affected by the disease, also showed sustained levels of CA activity above or equal

to those of WT controls at all time points, including at 12 months post treatment (Figures 2C and S1C). Interestingly, CA activity in the brain of treated mice at 7 days and 1 month post injection was 2–1.2 times higher than in the WT controls (Figures 2D and S1D). These results suggest that prolonged, high expression of the therapeutic enzyme in the liver may sustain the spread of PPCA into the brain, although it is still unclear how the protein would cross the blood-brain barrier. The pattern of expression of the PPCA protein in the liver, kidney, and brain of treated male and female mice largely reflected the pattern of CA activity measured in the same tissues (Figures S3A–S3F).

Restored CA activity in affected organs was paralleled by an increase in Neu1 activity that was equal to or greater than that measured in WT animals at all time points (Figures 2E–2H and S1E–S1H). Similarly, β -Gal activity, which tends to be at least two times higher than in WT controls in untreated *Ctsa*^{-/-} mice, was normalized in all tissues of AAV-injected mice, including the brain, at each time point (Figures 2I–2L and S1I–S1L). Last, treated mice showed a complete reversal of sialyl-oligosacchariduria up to 12 months post injection (Figure 3), confirming that restored expression of PPCA promotes the formation of a functional LMC.

Reversal of histopathology in AAV-treated *Ctsa*^{-/-} mice

Comparative histopathology of the liver, kidney, and spleen (Figures 4, 5, 6, and S4 and Tables S1 and S2) from treated and untreated *Ctsa*^{-/-} mice and WT controls was performed on H&E-stained sections. Montages of sequential images were stitched together to render a high-resolution composite image encompassing a large area of the individual tissues. The images of the *Ctsa*^{-/-} liver, comprising several lobules (Figure 4A and inset), highlighted the severe and widespread vacuolation of the hepatocytes, the endothelial cells of the sinusoids, and the Kupffer cells (Figure 4). In contrast, mice treated with scAAV2/8-CTSA showed complete normalization of the tissue architecture at 12 months post AAV injection (Figure S4A), which appeared nearly indistinguishable from that of the WT control (Figures 4B and 4C and insets). In agreement with the reversal of tissue morphology after treatment, immunohistochemistry (IHC) with anti-human PPCA antibody revealed high levels of expression of the protein in all affected cells, particularly those surrounding the blood vessels (Figure 4D and inset). The composite image of the *Ctsa*^{-/-} kidney from the cortex to the medulla (Figure 5A and inset) showed marked vacuolation of the convoluted tubular epithelium, the Bowman capsule and podocytes of the glomeruli, endothelial cells of the blood vessels in the cortex, and the ductal epithelium in the medulla. Occasional proteinaceous deposits were also visible (Figure 5A and inset). Despite being one of the most difficult organs to target by therapeutics, the kidney of treated mice also displayed extensive correction of tissue morphology, particularly evident in the cortex, whose appearance was comparable to that in the WT kidney (Figures 5B and 5C and insets; Figure S4B). Immunostaining of tissue sections demonstrated vast uptake of the PPCA precursor protein, especially in the cortex region by cells of the Bowman capsule and the proximal and distal tubular epithelium (Figure 5D and inset). The composite image of the *Ctsa*^{-/-} spleen (Figure 6A and inset) showed large areas of highly vacuolated splenocytes, primarily in the red pulp, most of

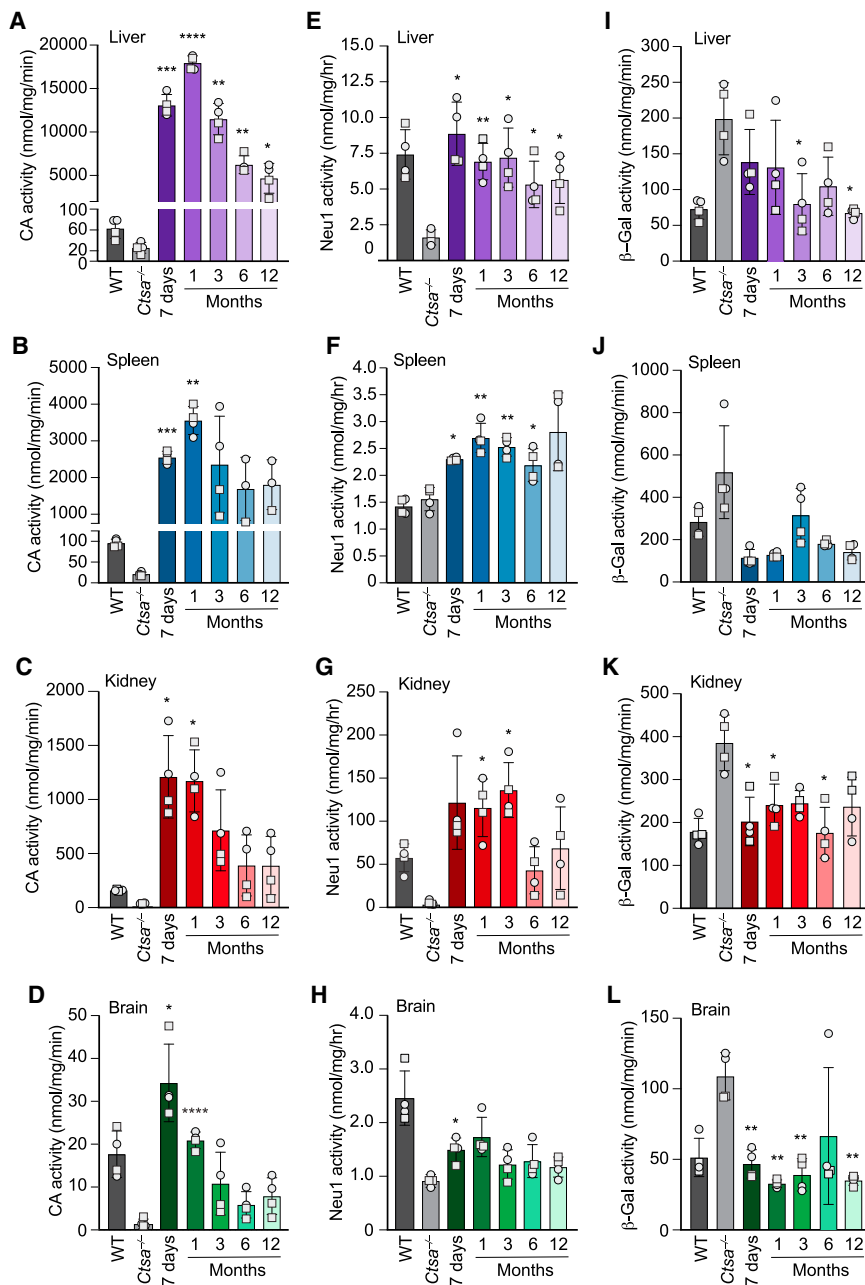


Figure 2. rhPPCA restores cathepsin A activity and corrects NEU1 and β -GAL activities in $Ctsa^{-/-}$ mice (A–D) Cathepsin A (CA) activity measured in (A) liver, (B) spleen, (C) kidney, and (D) brain lysates from $Ctsa^{-/-}$ mice treated with scAAV2/8-CTSA and collected 7 days and at 1, 3, 6, and 12 months following AAV-mediated gene transfer. (E–H) NEU1 and (I–L) β -GAL activities were measured in the same sets of tissues: (E and I) liver, (F and J) spleen, (G and K) kidney, and (H and L) brain. All the graphs are presented as mean \pm SD. Statistical analyses were performed using the Brown-Forsythe test; statistical differences between untreated and treated $Ctsa^{-/-}$ mice are indicated: * $p < 0.05$, ** $p < 0.01$, *** $p < 0.001$, **** $p < 0.0001$. Round symbols depict males, while square symbols depict females ($n \geq 3$).

stem, and the deep cerebellar nucleus (Figure 7). The protein was most efficiently internalized by the epithelial cells of the choroid plexus, which is a highly vascularized brain structure (Figure 7). These findings are potentially relevant from a therapeutic standpoint, although in order to translate them to the clinic, we would require further experiments in larger animal models.

Absence of neoplastic signs in the liver of AAV-treated $Ctsa^{-/-}$ mice

Given the potential risk for long-term AAV-treated mice to develop hepatocellular carcinoma,¹² we also surveyed multiple areas of the livers from treated $Ctsa^{-/-}$ mice at 12 months post injection. An example of a large, screened area of the tissue is shown in the H&E montage of Figure 4C. We could not detect any signs of abnormal morphology or growth, pleomorphism, aberrant trabeculae, and/or local infiltration in any of the liver tissues from the cohort of treated mice. In addition, we could not identify areas of ischemia, inflammation, or necrosis (Figure 4C).

Clinical chemistry and differential blood count in AAV-treated $Ctsa^{-/-}$ mice

We next performed a series of laboratory tests commonly used in the human population to obtain standardized, multiparametric, diagnostic measurements of blood samples and sera collected from all seven cohorts of mice (Table 1). The levels of amylase and glucose were used to assess pancreatic functionality (Table 2); the concentration of several electrolytes (calcium, phosphorus, potassium, and sodium) and the levels of blood urea nitrogen (BUN) and creatinine were indicative of kidney function (Table 2). In addition, to evaluate overall hepatic function and potential toxicity of high-dose AAV with sustained expression of the CTSA transgene in the liver, we tested a panel of liver-specific markers in the sera of treated and untreated mice (Table 2). Measured

them of histiocytic origin. Again, the morphology of the spleen of treated mice appeared entirely normalized, compared with the WT tissue (Figures 6B and 6C and insets; Figure S4C). Correction was particularly evident in the highly vascularized red pulp that also contained the highest number of PPCA-positive splenocytes (Figure 6D and inset).

Last, we were able to detect PPCA in the brain of treated mice at 12 months post injection (Figure 7). Scattered neurons and glia with punctate PPCA staining were detected in different brain regions, including the cortex, the cerebellum, the hippocampus, the brain

obtain standardized, multiparametric, diagnostic measurements of blood samples and sera collected from all seven cohorts of mice (Table 1). The levels of amylase and glucose were used to assess pancreatic functionality (Table 2); the concentration of several electrolytes (calcium, phosphorus, potassium, and sodium) and the levels of blood urea nitrogen (BUN) and creatinine were indicative of kidney function (Table 2). In addition, to evaluate overall hepatic function and potential toxicity of high-dose AAV with sustained expression of the CTSA transgene in the liver, we tested a panel of liver-specific markers in the sera of treated and untreated mice (Table 2). Measured

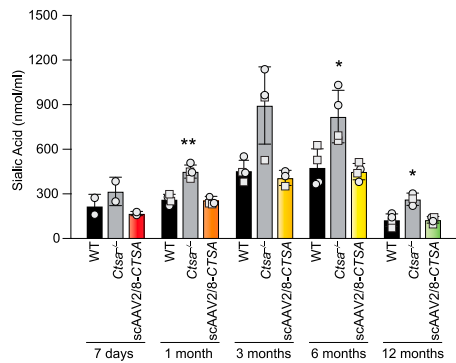


Figure 3. Sialy-oligosacchariduria reversal in scAAV2/8-CTSA-treated mice

Urinary sialic acid levels were measured 7 days and 1, 3, 6, and 12 months after AAV-mediated gene transfer. Data are presented as mean \pm SD. The dots in the graphical bars represent values obtained from each mouse. Statistical analyses were performed using the Brown-Forsythe test. * $p < 0.05$, ** $p < 0.01$. Round symbols depict males, while square symbols depict females ($n \geq 3$).

values of albumin, globulin, total bilirubin, total protein, and the liver enzymes alanine aminotransferase (ALT) and alkaline phosphatase (ALP) remained within normal range in all cohorts throughout the length of the treatment, further reiterating the safety and absence of toxicity following this therapeutic approach. Finally, we performed a differential blood count. We found no significant differences for values of hemoglobin, platelets, and hematocrit, as well as no statistically significant differences for absolute cell counts of neutrophils, lymphocytes, monocytes, eosinophils, basophils, and red blood cells in all the groups tested and at all time points post injection (Table 3).

Testing of antibody production against AAV2/8 capsid and human PPCA

One of the most encountered hurdles in AAV-mediated therapy is the risk that the recipient individual would mount an immune response toward the vector and/or the transgene product. This usually manifests with a weak innate immune response and a stronger adaptive immune response.^{13,14} The adaptive immune response involves the activation of both B cells that produce antibodies and cytotoxic T cells that ultimately kill infected cells. B cells can produce antibodies against the product of the transgene, but more often produce neutralizing antibodies against the viral capsid, which may prevent infection and therapeutic gene expression.^{14,15} Sera collected at 7 days and 1, 3, 6, and 12 months post injection were tested for the presence of antibodies against the viral capsid (AAV2/8) or against the human PPCA protein. These analyses showed the presence of antibodies against the virus at all time points (Figure 8A). Most importantly, no antibody response was detected against the human PPCA protein in any of the treated groups (Figure 8B). The presence of antibodies against the viral capsid may be due to the high titer of the vector employed in this study and/or the use of a self-complementary double-stranded AAV vector rather than a single-stranded vector.¹⁶ However, considering the widespread presence of the PPCA protein in all organs tested, the sustained CA activity throughout the duration of treat-

ment, and the normalization of all the pathological parameters at 12 months post injection, these antibodies did not seem to hamper the efficacy of the therapy.

Absence of T cell response to scAAV2/8-CTSA

To determine the immune-mediated toxicity that could occur during AAV-based therapy, we also measured interferon γ (IFN- γ) production and the relative percentage of CD4^{pos} and CD8^{pos} T cells in cultured splenocytes harvested from AAV-treated mice and re-exposed *in vitro* to the AAV virus. The IFN- γ ELISpot method, in conjunction with measurement of antibody production, is the most widely used technique to assess T cell immunity against multiple AAV serotypes.¹⁷ Splenocytes collected from WT and treated *Ctsa*^{-/-} mice (13 months) as well as untreated *Ctsa*^{-/-} mice (7 months) were cultured and re-infected with either scAAV2/8-CTSA or an empty scAAV2/8 vector. No significantly high levels of IFN- γ were measured in different splenocyte cultures, unless they were treated with the IFN- γ inducer phorbol 12-myristate 13-acetate (PMA)/ionomycin, used as positive control (Figure 8C). In addition, splenocyte cultures were used to assess the percentage of CD4^{pos} or CD8^{pos} T cells via flow cytometry (Figures S5A–S5D). No significant difference in the percentage of these T cells was detected among the different splenocyte cultures (Figures 8D and 8E), indicating that AAV treatment did not elicit a T-cell-mediated immune response.

DISCUSSION

In recent years, AAV-mediated gene therapy has become the preferred therapeutic method for LSD patients, and, as a result, several clinical trials have been approved by the Food and Drug Administration (FDA) and the European Medicines Agency (EMA). This effort has been spearheaded by the development of numerous AAV serotypes, isolated from humans, nonhuman primates, and other species.¹⁸ AAV2 was the first serotype to be vectorized and has been pseudo-typed using the capsids of other AAVs.¹⁹ This has expanded the cell types that can be infected by AAV, and, in turn, increased the efficacy of AAV-mediated gene therapy. An example of such engineering is the AAV we have used in this study, a pseudo-type of the AAV2 vector genome with the AAV8 capsid (designated AAV2/8), with enhanced tropism for hepatocytes.²⁰ Furthermore, efficient transduction depends on the binding of different AAV vectors to specific receptors and co-receptors present on target cells, which is again influenced by the specific AAV capsid.²¹

LSDs are particularly amenable to AAV-mediated gene therapy compared with other genetic diseases, because of the unique properties of many lysosomal enzymes to be secreted into the circulation as inactive or partially active precursors and, then, recaptured by neighboring or distant cells via receptor-mediated endocytosis.²² Thus, AAV-infected deficient cells can become producers of the therapeutic enzyme that, when secreted, cross-corrects other deficient cells and, in turn, reverts the pathologic manifestations inherent to the disease. AAV-mediated, *in vivo* gene therapy has been implemented in several LSD models and patients for the treatment of GM1 gangliosidosis, mucopolysaccharidosis type I (MPSI) and MPSIIIB, Sandhoff disease,

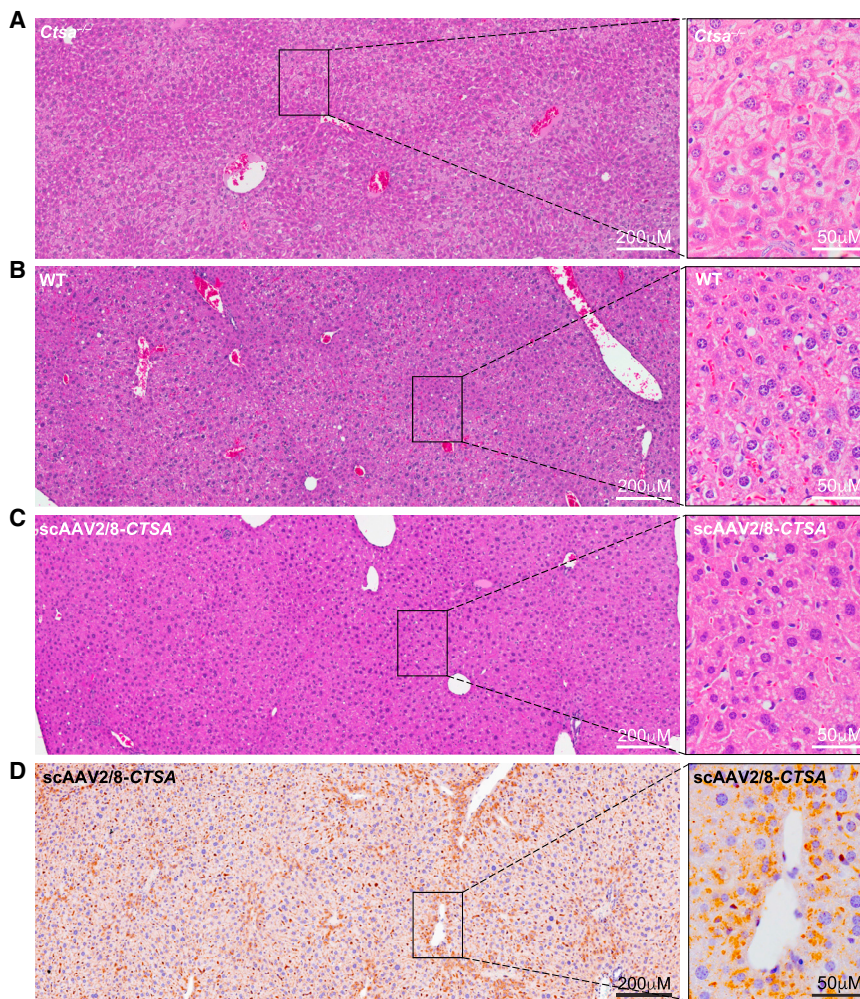


Figure 4. Complete restoration of liver morphology in scAAV2/8-CTSA

Composite images of H&E-stained sections show extensive vacuolization in the liver of untreated *Ctsa*^{-/-} mice (A and inset), but a complete clearance and restoration to WT morphology in animals treated with scAAV2/8-CTSA (B, wild type; C, scAAV2/8-CTSA; and insets). (D and inset) Representative composite of IHC images performed on the liver of scAAV2/8-CTSA-treated mice using a human PCCA-specific antibody. Brown punctate staining depicts compartmentalized/lysosomal PCCA staining.

metachromatic leukodystrophy, and Krabbe disease.²³ However, only a few reports are present in the literature that have addressed the potential side effects of long-term overexpression of a therapeutic enzyme and/or high vector dose.^{24–26} Here, we have exploited the therapeutic potential of PCCA for the treatment of GS by investigating the effect of a high-dose scAAV2/8-CTSA vector in *Ctsa*^{-/-} mice, expressing the transgene from a liver-specific promoter. The intent of the study was to evaluate not only the efficacy of the treatment in correcting several disease-specific phenotypes, but also the potential toxicity associated with a high dose of the AAV vector and/or overexpression of the CTSA transgene, including the mounting of an immune response.

Overcoming the host immune response is indispensable for the successful treatment of LSDs in patients, since it can seriously hamper the safety and efficacy of this gene therapy approach. The host may elicit both humoral and cellular immune responses by activating antigen-specific CD4^{pos} helper and/or CD8^{pos} cytotoxic T cells, and by producing antibodies against the viral capsid and/or the transgene product. Capsid-neutralizing antibodies have been detected following

AAV-mediated gene therapy with detrimental effects on treatment outcome, as was reported in preclinical studies carried out in animal models of Pompe disease and hemophilia B.^{27–29} Surprisingly, in our current study, we have detected antibodies only against the viral capsid, not the PCCA transgene product, despite the fact that our mouse model is a total knockout. This indicates that the human PCCA protein is not particularly immunogenic in this experimental setting, as was observed previously using other therapeutic approaches in the same mouse model.^{5,7–9} In addition, the lack of neutralizing antibodies against PCCA explains the sustained expression of the transgene at 12 months post injection. These results should also take into account the intrinsic characteristics of the PCCA protein, which is secreted as a zymogen, is readily internalized by deficient cells, and is stable in tissues. In contrast, in a human clinical trial for hemophilia B, which employed the identical AAV backbone used in this study, intravenous injection of a scAAV2/8.LP1.hcoFIX vector resulted in a long-lasting (>5 years) increase in plasma FIX (from <1% to 1%–8%), but the patients developed antibodies against AAV capsid epitopes.³⁰ In addition, and again contrary to our observations, elevated transaminases were measured at 7–10 weeks post AAV injection, and the patients needed to be treated with corticosteroids to normalize their levels.³¹ Most likely, the combination of persistent liver insult and the strong immune response against the AAV capsid contributed to the clearance of 50%–70% in plasma FIX.³¹ Although we cannot compare our mouse study with the aforementioned human clinical trial, we can postulate that the persistent expression of the PCCA transgene for up to 12 months post injection is indeed attributable to the nonimmunogenic and nontoxic nature of the protein. This also explains why there is no activation of antigen-specific CD4^{pos} helper and/or CD8^{pos} cytotoxic cells and no detectable liver inflammation.

The results of these studies are also relevant in light of recent reports that link high doses of AAV particles to acute liver failure and shock in nonhuman primates as well as proprioceptive ataxia in pigs.^{32,33}

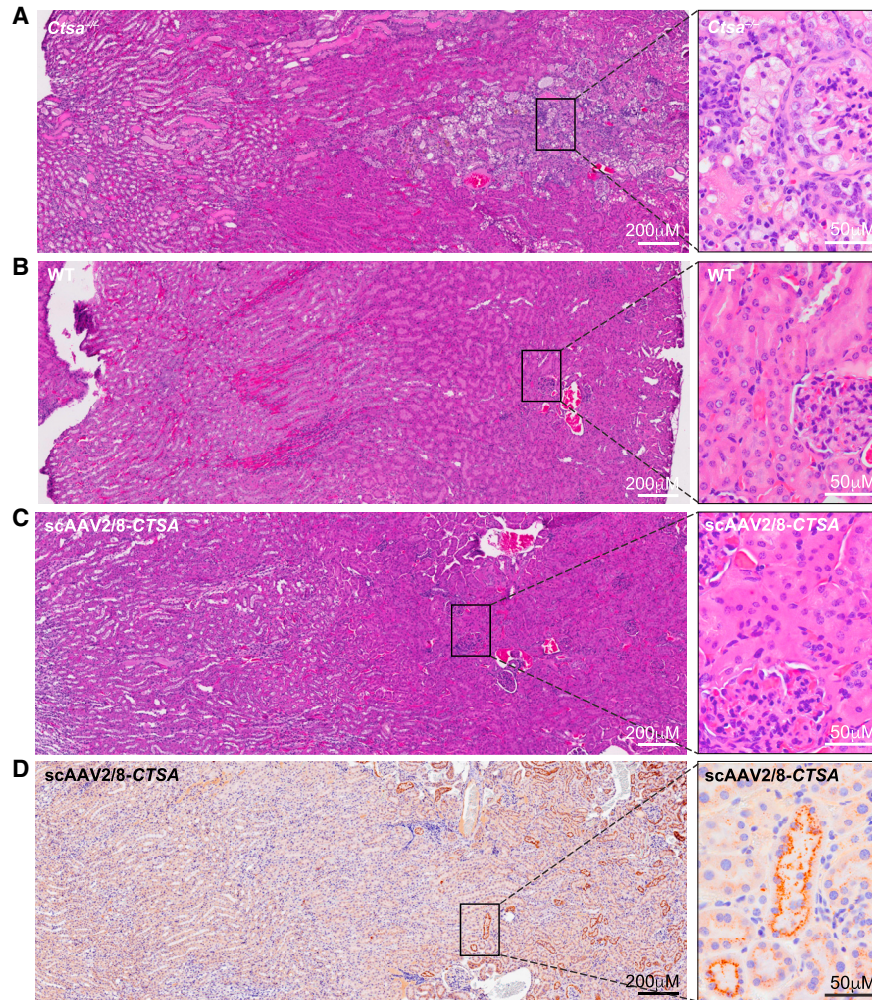


Figure 5. Extensive correction of kidney morphology in scAAV2/8-CTSA-treated mice

Montage of images of H&E-stained sections shows extensive disruption of kidney architecture in untreated *Ctssa*^{-/-} mice (A and inset), but a nearly full improvement of tissue morphology similar to WT morphology in animals treated with scAAV2/8-CTSA (B, wild type; C, scAAV2/8-CTSA; and insets). (D and inset) Representative composite of IHC images performed on the kidney of AAV2/8-treated *Ctssa*^{-/-} mice using a human PPCA-specific antibody. Brown punctate staining depicts compartmentalized/lysosomal PPCA staining.

Although AAV gene therapy seems to be the elected therapeutic choice for LSDs, a few studies have raised concerns about the use of recombinant AAV as a gene transfer vector because of evidence of AAV integration in the host cells.^{34–37} This could occur within or in the proximity of oncogenes, potentially promoting malignant transformation. Several reports have described integration of AAV into the RNA imprinted and accumulated in nucleus (Rian) locus or near growth-regulatory genes, following long-term gene therapy.³⁸ These integration events have been linked to the development of hepatocellular carcinoma (HCC). For example, in a preclinical gene therapy study performed in a canine model of factor VIII deficiency, nine dogs were followed for 10 years. Analysis of integration sites in liver samples from six treated dogs identified more than 1,700 AAV integration events in the genomic DNA, with a considerable percentage of these

in the vicinity of regulatory genes, resulting in hyperplasia of liver cells in five dogs.³⁹ Adding to these concerns is the high incidence of HCC observed in a murine model of Krabbe disease after CNS-directed therapy.⁴⁰ Although worrisome, the occurrence of HCC seems to depend on several contributing factors, i.e., the very high dose of AAV vector, the use of strong promoter/enhancer elements, the starting of treatment during the neonatal period, and, most importantly, liver damage/inflammation.¹² These “predisposing factors” have been implicated in increased occurrence of HCC⁴¹ in mice with nonalcoholic fatty liver disease or liver injury that have been treated with AAV-based therapy, targeting the Rian locus. This is also in line with an occurrence of HCC in a hemophilic patient treated with AAV5-FIX,⁴² which has halted a clinical trial for hemophilia managed by the company uniQure. As in the case of the murine study, the patient had multiple risk factors

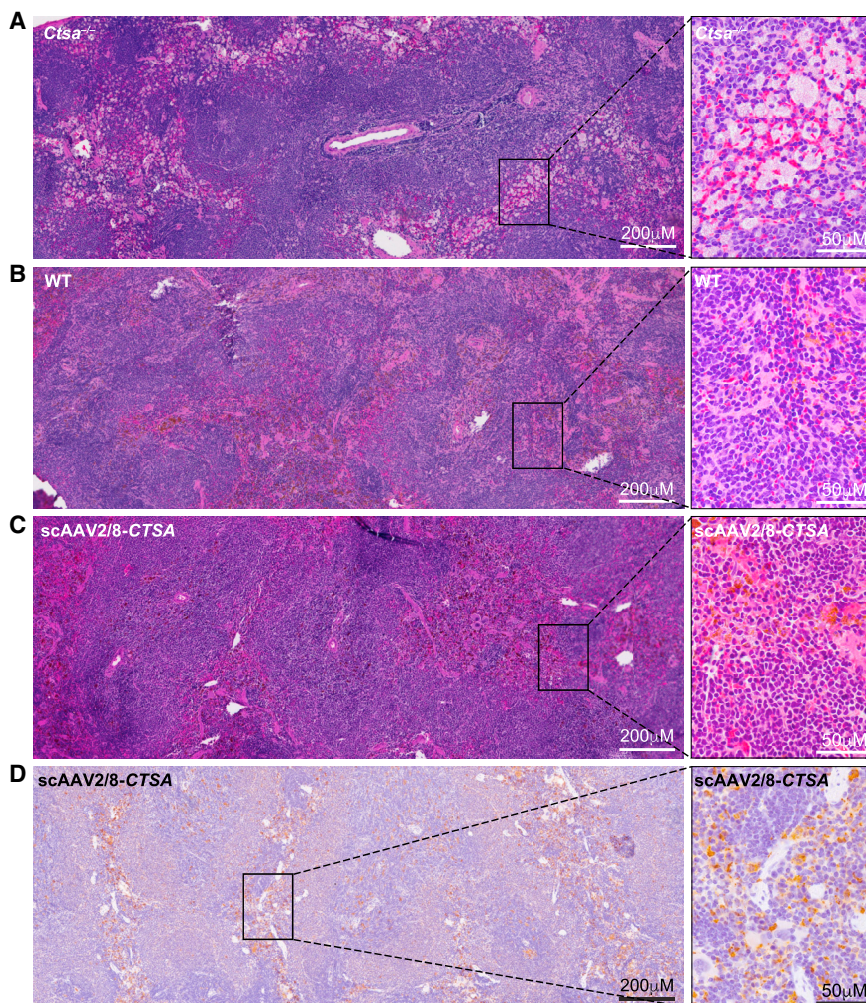


Figure 6. Normalization of spleen architecture in scAAV2/8-CTSA-treated mice

Montage of images of H&E-stained sections shows extensive ballooning of splenocytes in untreated *Ctsa*^{-/-} mice (A and inset), but resolution of cell vacuolation and complete normal morphology similar to WT in animals treated with scAAV2/8-CTSA (B, wild type; C, scAAV2/8-CTSA; and insets). (D and inset) Representative composite of IHC images performed on the spleen of injected animals using a human PCCA-specific antibody. Brown punctate staining depicts compartmentalized/lysosomal PCCA staining.

associated with HCC, including a history of hepatitis C and hepatitis B and evidence of nonalcoholic fatty liver disease.

It is, however, reassuring that a very recent prospective study in mouse and cat models of MPSVI treated at young adult age and at postnatal day 50, respectively, with a high-dose, single-stranded AAV2/8 vector expressing human arylsulfatase B in the liver found low incidence of HCC.²⁵ In line with this study, we found no evidence of liver injury or inflammation, as well as no detectable HCC for up to 12 months after scAAV2/8-CTSA-mediated therapy.

In conclusion, the high-efficacy and low-toxicity results of this pre-clinical study provide a strong rationale for implementing AAV-mediated *in vivo* gene therapy in the treatment of patients with GS.

MATERIALS AND METHODS

Study design

The *Ctsa*^{-/-} model has been extensively used in several preclinical studies to test various therapeutic approaches, and no clear gender

bias to treatment has been observed. In addition, because the males are infertile and the crossing of heterozygotes produces small litters with often a limited number of *Ctsa*^{-/-} mice, we were allowed by an FDA pre-IND panel to reduce the number of animals in compliance with the 3R guiding principles for animal experimentation.⁴³ A total of 28 mice were used in this study. They were divided into seven groups, composed of four mice each, two males and two females. Four *Ctsa*^{-/-} mice in each group received a dose of scAAV2/8-LP1-hCTSA (scAAV2/8-CTSA) at 2×10^{13} vg/kg administered via tail vein at 1 month of age and were sacrificed 7 days and 1, 3, 6, and 12 months post injection. Two male and two female WT and *Ctsa*^{-/-} mice were used as controls in each group. Liver, lung, spleen, heart, kidney, pancreas, testis, epididymis or uterus and ovary, diaphragm, jejunum, inguinal lymph nodes, and brain were collected

for enzymatic activities and immunohistochemistry and bio-distribution analyses and were either snap-frozen in liquid nitrogen or fixed in 10% neutralized formalin and paraffin embedded. Blood and urine were collected at all time points. Sera were used for the clinical chemistry and complete blood count (CBC) panels and antibody response; urine was used for sialic acid content analyses.

Animals

Animals were housed in a fully Association for Assessment and Accreditation of Laboratory Animal Care (AAALAC)-accredited animal facility with controlled temperature (22°C), humidity, and lighting (alternating 12-h light/dark cycles). Food and water were provided *ad libitum*. All procedures in mice were performed according to animal protocols approved by the St Jude Children's Research Hospital Institutional Animal Care and Use Committee and National Institutes of Health guidelines. All experiments were performed in *Ctsa*^{-/-} mice and WT littermate controls in the FVB background.

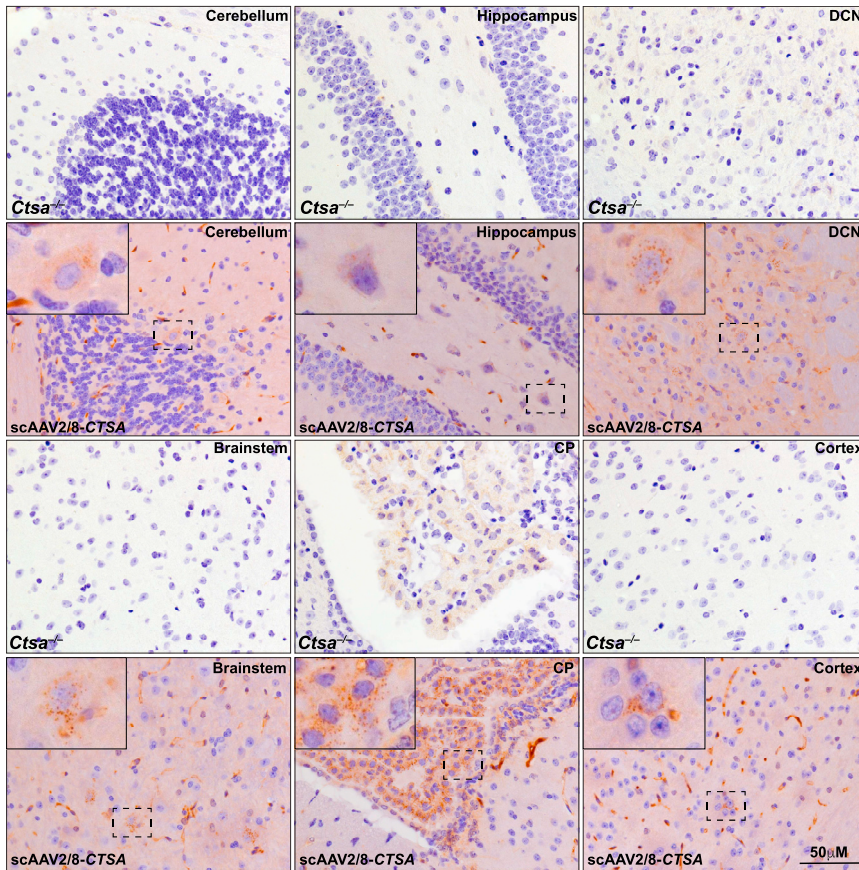


Figure 7. Detection of PPCA in the brain of scAAV2/8-CTSA-treated mice

Representative IHC images using a human PPCA-specific antibody in several regions of the brain of injected animals. Corresponding brain regions of untreated *Ctsa*^{-/-} mice are shown for comparison. Brown punctate staining depicts compartmentalized/lysosomal PPCA staining. CP, choroid plexus; DCN, deep cerebellar nucleus.

measured against the dipeptide Z-Phe-Ala (Sigma, St. Louis, MO, USA), Neu1 catalytic activity was measured against synthetic 4-methylumbelliferyl- α -D-N-acetylneuraminic acid (Sigma, St. Louis, MO, USA), and β -GAL was measured against 4-methylumbelliferyl- β -D-galactopyranoside (Sigma, St. Louis, MO, USA). All reactions were performed at 37°C for 1 h and stopped with carbonate stop buffer (0.5 M Na₂CO₃ with the pH set to 10.7 by adding 0.5 M NaHCO₃) for Neu1 and β -GAL activities, while the CA activity was stopped at 100°C for 5 min, and 10 μ L reaction mixture was read in 250 μ L 50 mM sodium-carbonate stop buffer (pH 9.5), containing 500 μ L o-phthalaldehyde (10 mg/mL) and 500 μ L 2-mercaptoethanol (5 μ L/mL) per 30 mL. Fluorescence was measured at λ_{ex} 355/ λ_{em} 460 and interpolated to a standard curve adjusted for dilution and normalized to protein concentration.

measured against the dipeptide Z-Phe-Ala (Sigma, St. Louis, MO, USA), Neu1 catalytic activity was measured against synthetic 4-methylumbelliferyl- α -D-N-acetylneuraminic acid (Sigma, St. Louis, MO, USA), and β -GAL was measured against 4-methylumbelliferyl- β -D-galactopyranoside (Sigma, St. Louis, MO, USA). All reactions were performed at 37°C for 1 h and stopped with carbonate stop buffer (0.5 M Na₂CO₃ with the pH set to 10.7 by adding 0.5 M NaHCO₃) for Neu1 and β -GAL activities, while the CA activity was stopped at 100°C for 5 min, and 10 μ L reaction mixture was read in 250 μ L 50 mM sodium-carbonate stop buffer (pH 9.5), containing 500 μ L o-phthalaldehyde (10 mg/mL) and 500 μ L 2-mercaptoethanol (5 μ L/mL) per 30 mL. Fluorescence was measured at λ_{ex} 355/ λ_{em} 460 and interpolated to a standard curve adjusted for dilution and normalized to protein concentration.

scAAV2/8-CTSA vector production and titration

The production and titration of the scAAV2/8-CTSA construct have been previously described.⁷ The scAAV vector particles were made using a good manufacturing practice (GMP) process, comparable to the transient-transfection procedure in the Children's GMP, LLC, facility on the St Jude campus, as previously described for the hemophilia B vector.⁴⁴

Biodistribution

Genomic DNA was extracted from liver, lung, heart, kidney, pancreas, testis, epididymis or uterus and ovary, diaphragm, jejunum, inguinal lymph nodes, and brain by using the DNeasy Blood and Tissue Kit (Qiagen, Germantown, MD, USA), following the manufacturer's guidelines. qRT-PCR was performed using a primer set spanning the LP1 promoter and the PPCA gene insert. A standard curve with known copy number was used to determine the concentration in all tissues tested. Results were plotted as copy number/ μ g DNA.

Cathepsin A, Neu1, and β -GAL activity assays

Snap-frozen liver, spleen, kidney, and brain samples isolated from WT, untreated, and treated *Ctsa*^{-/-} mice from each group were homogenized on ice in three volumes of water (w/v) using the Qiagen TissueLyser II (Qiagen, Germantown, MD, USA). CA activity was

Uptake of PPCA zymogen in patients' fibroblasts

A total of 1.5×10^5 GS and control fibroblasts were seeded into six-well plates in duplicate and cultured until 90% confluency. Fibroblasts were grown at 37°C in Dulbecco's modified Eagle's medium (DMEM) supplemented with 10% fetal bovine serum (FBS) (BioWest), 2 mM GlutaMAX, penicillin (100 U/mL), and streptomycin (100 μ g/mL) (Gibco) in a humidified 5% CO₂ atmosphere. Fifty microliters of sera collected from three treated *Ctsa*^{-/-} mice (S1, S2, and S3) and 100 μ L collected from a WT mouse were added in 1 mL fresh medium to the wells containing GS fibroblasts. After 60 h, the cells were rinsed extensively with PBS, collected, and lysed in H₂O containing 0.5% Tween 20 (3 \times) and incubated on ice for 30 min, with mixing every 10 min by vortex. Both untreated WT and GS fibroblasts were used as controls. The CA and NEU1 activity assays were performed as described above. The fluorescence was measured (λ_{ex} 355/ λ_{em} 460), and the specific enzyme activities were calculated. NEU1 activities were calculated as nanomoles of substrate converted per milligram of protein per hour (nmol/mg/h), whereas the CA activities were calculated as picomoles of substrate converted per milligram of protein per minute (pmol/mg/min).

Table 2. Comprehensive metabolic panel

	Range ^a /unit		7 days	1 month	3 months	6 months	12 months
Pancreatic function							
Amylase	602–2,311	WT	1,175 ± 88	1,529 ± 252	1,452 ± 65	1,844 ± 671	1,394 ± 352
	U/L	<i>Ctsa</i> ^{-/-}	1,153 ± 154	1,405 ± 320	1,774 ± 575	1,955 ± 315	2,494 ± 384
		scAAV2/8-CTSA	1,778 ± 592	1,552 ± 186	1,642 ± 237	1,305 ± 226	1,772 ± 762
Glucose	106–278	WT	294 ± 36	267 ± 42	245 ± 40	208 ± 42	219 ± 49
	mg/dL	<i>Ctsa</i> ^{-/-}	253 ± 58	265 ± 36	193 ± 31	219 ± 43	100 ± 51
		scAAV2/8-CTSA	179 ± 63	242 ± 43	177 ± 58	208 ± 45	238 ± 15
Renal function (electrolytes)							
Calcium	9–12	WT	10.2 ± 0.16	10.6 ± 1.98	10.7 ± 0.10	9.4 ± 1.12	15.9 ± 1.54
	mg/dL	<i>Ctsa</i> ^{-/-}	11.3 ± 0.77	10.5 ± 0.64	9.5 ± 0.38	9.7 ± 0.80	11.2 ± 2.04
		scAAV2/8-CTSA	10.6 ± 1.12	10.8 ± 1.02	8.7 ± 1.81	9.3 ± 1.06	13.1 ± 0.93
Phosphorus	6–13	WT	12.8 ± 0.30	10.4 ± 1.23	8.43 ± 0.92	10.5 ± 1.25	12.9 ± 2.97
	mg/dL	<i>Ctsa</i> ^{-/-}	15.6 ± 1.70	11.0 ± 0.60	10.8 ± 2.85	10.0 ± 0.69	12.6 ± 2.35
		scAAV2/8-CTSA	13.5 ± 1.74	9.93 ± 0.86	8.10 ± 0.96	11.3 ± 0.55	10.8 ± 1.30
Potassium	5–9	WT	9.7 ± 0.43	9.2 ± 1.2	7.6 ± 0.57	9.6 ± 1.5	10.0 ± 2.6
	mmol/L	<i>Ctsa</i> ^{-/-}	12 ± 1.9	9.3 ± 1.9	10 ± 0.63	9.6 ± 0.77	7.9 ± 1.5
		scAAV2/8-CTSA	11 ± 2.3	7.4 ± 0.0	7.3 ± 0.57	10 ± 0.41	11 ± 1.9
Sodium	147–167	WT	143 ± 1.2	151 ± 7.7	139 ± 1.5	152 ± 8.7	142 ± 2.2
	mmol/L	<i>Ctsa</i> ^{-/-}	147 ± 4.2	144 ± 5.5	148 ± 2.8	144 ± 8.5	148 ± 17
		scAAV2/8-CTSA	147 ± 3.1	141 ± .00	132 ± 8.5	138 ± 13	152 ± 7.7
Renal function							
Blood urea nitrogen (BUN)	19–34	WT	25.5 ± 4.8	28.1 ± 6.0	28.5 ± 3.5	24.0 ± 1.5	25.5 ± 6.7
	mg/dL	<i>Ctsa</i> ^{-/-}	26.2 ± 1.5	24.8 ± 3.0	27.0 ± 2.1	29.5 ± 5.5	51.4 ± 22.6
		scAAV2/8-CTSA	27.2 ± 4.4	26.5 ± 4.4	28.7 ± 7.2	27.6 ± 11.4	28.3 ± 2.6
Creatinine	0.5–0.8	WT	0.33 ± 0.10	0.42 ± 0.16	0.35 ± 0.12	0.25 ± 0.10	0.20 ± 0.04
	mg/dL	<i>Ctsa</i> ^{-/-}	0.18 ± 0.12	0.60 ± 0.01	0.36 ± 0.21	0.33 ± 0.11	0.38 ± 0.14
		scAAV2/8-CTSA	0.25 ± 0.08	0.32 ± 0.12	0.30 ± 0.15	0.24 ± 0.04	0.24 ± 0.09
Hepatic function							
Albumin	2.6–4.6	WT	2.95 ± 0.10	3.00 ± 0.00	3.25 ± 0.13	3.05 ± 0.30	3.00 ± 0.43
	g/dL	<i>Ctsa</i> ^{-/-}	3.20 ± 0.28	3.23 ± 0.32	2.80 ± 0.16	2.65 ± 0.34	2.00 ± 0.50
		scAAV2/8-CTSA	2.60 ± 0.37	3.13 ± 0.15	3.15 ± 0.41	2.80 ± 0.43	2.60 ± 0.87
Globulin	2.2–2.6	WT	2.40 ± 0.16	2.73 ± 1.03	2.78 ± 0.17	2.65 ± 0.38	2.35 ± 0.62
	g/dL	<i>Ctsa</i> ^{-/-}	2.20 ± 0.52	2.30 ± 0.46	2.50 ± 0.58	2.45 ± 0.34	1.90 ± 0.86
		scAAV2/8-CTSA	2.60 ± 0.98	2.75 ± 0.21	3.80 ± 0.49 ^b	2.75 ± 0.38	2.65 ± 0.57
Total bilirubin	0.3–0.8	WT	1.50 ± 0.58	0.53 ± 0.33	0.62 ± 0.51	0.60 ± 0.26	1.30 ± 0.13
	mg/dL	<i>Ctsa</i> ^{-/-}	0.92 ± 0.62	0.68 ± 0.14	0.38 ± 0.23	0.61 ± 0.16	0.63 ± 0.66
		scAAV2/8-CTSA	0.78 ± 0.64	0.62 ± 0.39	0.39 ± 0.19	1.10 ± 0.42	1.30 ± 0.18
Total protein	4.3–6.4	WT	5.5 ± 0.25	6.3 ± 1.30	6.0 ± 0.15	5.7 ± 0.62	5.4 ± 0.97
	g/dL	<i>Ctsa</i> ^{-/-}	5.4 ± 0.78	5.6 ± 0.29	5.3 ± 0.38	5.1 ± 0.66	4.5 ± 1.80
		scAAV2/8-CTSA	5.3 ± 0.60	5.9 ± 0.21	6.9 ± 0.89	5.6 ± 0.81	6.1 ± 0.93
Alanine Aminotransferase (ALT)	26–120	WT	43.5 ± 15	136 ± 79	116.0 ± 30	45.5 ± 18	45.0 ± 21
U/L	<i>Ctsa</i> ^{-/-}	22.5 ± 19	95.7 ± 27	101.0 ± 78	37.5 ± 6.8	61.5 ± 46	
	scAAV2/8-CTSA	104.0 ± 69	140.0 ± 39	88.7 ± 9.5	52.0 ± 9.2	33.0 ± 20	

(Continued on next page)

Table 2. Continued

	Range ^a /unit		7 days	1 month	3 months	6 months	12 months
Alkaline phosphatase (ALP)	44–118	WT	186 ± 17	187 ± 99	144 ± 23	58 ± 15	90 ± 20
	U/L	<i>Ctsa</i> ^{-/-}	251 ± 30	173 ± 35	124 ± 50	71 ± 7	80 ± 49
		scAAV2/8-CTSA	299 ± 33 ^b	223 ± 26	124 ± 12	90 ± 23	82 ± 26

^aThe range is based on data from mice ages 6–8 weeks provided by St Jude Children's Research Hospitals Veterinary Pathology Core.

^bValues in treated animals that show statistical difference from the WT group, $p < 0.05$.

Sialic acid content assay

The total sialyl-oligosaccharide content in mouse urine was determined by the release of bound sialic acid using an EnzyChrom Sialic Acid Assay Kit (ESLA-100, Bioassay Systems, Hayward, CA, USA). Total sialic acid was measured following acid hydrolysis for 1 h at 80°C. After the addition of neutralization buffer, samples were set to cool at room temperature (RT) and incubated with an enzymatic master mix to utilize an enzyme-coupled reaction to oxidize any liberated sialic acid. A standard curve was generated from a 10 mM sialic acid stock solution that was serially diluted in ultra-pure water. The fluorescence was read at λ_{ex} 535 nm and λ_{em} 595 nm. Results were interpolated to a standard curve and presented as micromolar (nmol/mL) sialic acid.

Immunohistochemical analyses

Six-micrometer-thick paraffin-embedded tissue sections were subjected to deparaffinization and antigen retrieval using pressure cooker methods, according to the manufacturer's instructions (Prestige Medical, Los Angeles, CA, USA). After being blocked with 0.1% bovine serum albumin and 0.5% Tween 20 in PBS, the sections were incubated overnight at RT with anti-hPPCA antibody (generated in-house). Sections were rinsed in PBS and subsequently incubated with biotinylated secondary goat anti-rabbit antibody (Jackson ImmunoResearch Laboratory, West Grove, PA, USA) for 1 h. Endogenous peroxidase was quenched by incubating the sections with 3% hydrogen peroxidase for 15 min. Antibody detection was performed using the ABC Kit (Vector Laboratories, Burlingame, CA, USA) and diaminobenzidine substrate (Invitrogen). Sections were counterstained with hematoxylin, according to the standard method. For histopathological examination, 6- μm -thick sections were stained with a standard H&E method and analyzed blindly. To measure the extent of vacuolation in sections from liver, spleen, and kidney, a macro was developed in ImageJ to analyze the total area occupied by vacuoles. A threshold for detection was set for each tissue and batched to all images using the same parameters. The total vacuolation area was normalized to that measured in WT samples.

Clinical chemistry and complete blood count panels

Whole blood samples (~250 μL) were collected at different time points from WT, untreated, and treated *Ctsa*^{-/-} mice in tubes containing 15 μL EDTA. Clinical chemistry and CBC panels were performed by the Veterinary Pathology Core of St Jude Children's Research Hospital.

Detection of antibodies against AAV2/8 capsid and human PPCA transgene product

Antibody levels were tested in the sera of WT, untreated, and treated *Ctsa*^{-/-} mice via an enzyme-linked immunosorbent assay (ELISA). Serum was used for the ELISA. Briefly, either disrupted scAAV2/8-CTSA virus or purified PPCA protein was diluted to 1 $\mu\text{g}/\text{mL}$ in DPBS at 50 μL per well in a Nunc MaxiSorp ELISA plate. When purified virus was used, virus concentration was estimated using bicinchoninic acid (BCA) assay prior to disruption. The virus stock was incubated in disruption buffer containing 5 mM Tris (pH 7.8), 60 mM KCl, and 0.05% Triton X-100 for 15 min at RT. Virus was then diluted in DPBS to 1 $\mu\text{g}/\text{mL}$. A human-specific PPCA antibody was used as positive control for the ELISA against PPCA. Plates were incubated at 4°C overnight to allow the protein/virus to bind. Following incubation, the plates were washed twice with DPBS/0.05% Tween 20 (washing buffer) and blocked with 10% FBS in DPBS (blocking buffer) for 30 min at RT. Plates were washed twice with washing buffer, and diluted samples in triplicate were placed in the wells for 2 h. Plates were then washed twice with washing buffer, and goat anti-mouse immunoglobulin G-horseradish peroxidase (IgG-HRP) (Southern Biotechnology, Birmingham, AL, USA) was used as a secondary antibody diluted 1:5,000 in blocking buffer. Plates were incubated for 1 h at RT and washed three times with washing buffer, and TMB 2-Component Microwell Peroxidase Substrate (SeraCare Life Sciences, Gaithersburg, MD, USA) was added to each well. Plates were allowed to develop for 15 min, and the reaction was stopped by adding an equal volume of 1 M phosphoric acid. Plates were then read in a Molecular Devices Spectramax M5 at an OD of 450. Triplicates were averaged and plotted.

Interferon- γ ELISpot

The ELISpot 96-well plate was washed four times with sterile PBS (200 $\mu\text{L}/\text{well}$). The plate was then conditioned with culture medium (DMEM supplemented with 10% FBS, 1 \times Pen-Strep, and 1 \times Gluta-MAX) (200 $\mu\text{L}/\text{well}$) and incubated at RT for 30 min. Splenocytes were then resuspended into 1-mL aliquots, each containing 1.5×10^6 cells. These aliquots were spun down in a microcentrifuge at 1,500 rpm for 5 min followed by resuspension in 600 μL of medium containing: (1) 100 MOI of scAAV2/8-CTSA with a titer of 4.0×10^{12} gc/mL, (2) 100 MOI of empty AAV capsid with a titer of 2.5×10^{13} gc/mL, or (3) 40.5 nM PMA plus 670 nM ionomycin or (4) medium only. Conditioning medium was removed from the plate and replaced with 200 $\mu\text{L}/\text{well}$ of stimulus medium, containing 500,000 cells. Each sample was plated in triplicate, and the plate was incubated at 37°C with 5%

Table 3. Complete blood count

	Units	Range ^a		7 days	1 month	3 months	6 months	12 months
Hemoglobin	g/dL	10.9–13.0	WT	13.0 ± 0.5	13.8 ± 0.6	12.0 ± 0.5	12.5 ± 0.5	13.9 ± 0.6
			<i>Ctsa</i> ^{-/-}	13.2 ± 0.9	13.2 ± 0.9	12.1 ± 0.5	11.3 ± 0.3	9.9 ± 2.3
			scAAV2/8-CTSA	13.3 ± 0.4	12.7 ± 0.5	13.1 ± 0.4	11.6 ± 1.0	12.7 ± 0.8
Platelets	×10 ³ /μL	706.5–988.2	WT	725 ± 43	567 ± 69	701 ± 90	634 ± 24	736 ± 56
			<i>Ctsa</i> ^{-/-}	689 ± 104	546 ± 181	469 ± 91	672 ± 15	616 ± 103
			scAAV2/8-CTSA	771 ± 137	533 ± 26	657 ± 54	485 ± 53	641 ± 25
Hematocrit	%	36.3–44.5	WT	42 ± 1.1	47 ± 2.4	43 ± 2.1	46 ± 1.6	49 ± 3.0
			<i>Ctsa</i> ^{-/-}	50 ± 1.5	47 ± 2.0	44 ± 2.5	44 ± 1.1	33 ± 6.3
			scAAV2/8-CTSA	50 ± 1.5	45 ± 2.0	47 ± 1.3	38 ± 2.7	44 ± 2.1
White blood cells	×10 ³ /μL	2.0–6.5	WT	5.1 ± 0.92	7.2 ± 3.3	3.5 ± 0.45	4.6 ± 0.7	4.6 ± 0.85
			<i>Ctsa</i> ^{-/-}	6.8 ± 1.7	11.0 ± 3.2	9.5 ± 2.9	4.3 ± 0.79	2.3 ± 0.89
			scAAV2/8-CTSA	7.5 ± 2.2	9.5 ± 1.7	5.3 ± 1.0	6.0 ± 1.7	4.4 ± 0.82
Neutrophils	%	16.7–24.6	WT	33.4 ± 2.2	21.3 ± 3.8	19.1 ± 4.3	29.5 ± 3.7	40.5 ± 10.9
			<i>Ctsa</i> ^{-/-}	31.2 ± 2.8	20.5 ± 4.2	22.9 ± 5.2	38.2 ± 8.7	44.9 ± 7.3
			scAAV2/8-CTSA	24.4 ± 5.6	21.4 ± 7.0	26.6 ± 4.6	25.6 ± 1.9	31.1 ± 4.0
Lymphocytes	%	62.1–73.9	WT	55.5 ± 2.7	67.1 ± 10.8	78.1 ± 5.5	59.3 ± 5.7	53.2 ± 7.2
			<i>Ctsa</i> ^{-/-}	54.6 ± 2.1	72.2 ± 6.4	67.8 ± 9.0	52.8 ± 7.2	51.0 ± 7.0
			scAAV2/8-CTSA	62.1 ± 10.3	68.6 ± 6.3	65.6 ± 4.6	60.2 ± 1.7	60.1 ± 5.7
Monocytes	%	6.2–14.5	WT	9.92 ± 1.3	7.57 ± 0.5	3.34 ± 1.91	9.41 ± 1.4	5.63 ± 4.1
			<i>Ctsa</i> ^{-/-}	10.8 ± 2.2	6.24 ± 1.0	8.07 ± 2.9	8.23 ± 1.7	2.98 ± 1.7
			scAAV2/8-CTSA	9.04 ± 2.2	9.28 ± 0.7	7.59 ± 0.2	10.5 ± 1.6	7.37 ± 1.6
Eosinophils	%	0.03–0.4	WT	0.89 ± 0.6	0.36 ± 0.4	0.05 ± 0.05	1.42 ± 1.2	0.48 ± 0.3
			<i>Ctsa</i> ^{-/-}	2.26 ± 0.7	0.59 ± 0.9	0.79 ± 1.3	0.38 ± 0.3	0.77 ± 1.2
			scAAV2/8-CTSA	1.43 ± 1.1	0.73 ± 0.6	0.23 ± 0.3	2.4 ± 1.8	1.21 ± 1.3
Basophils	%	0.05–0.4	WT	0.26 ± 0.2	0.13 ± 0.1	0.02 ± 0.03	0.45 ± 0.6	0.23 ± 0.3
			<i>Ctsa</i> ^{-/-}	1.20 ± 0.2	0.45 ± 0.5	0.38 ± 0.4	0.40 ± 0.4	0.33 ± 0.6
			scAAV2/8-CTSA	0.52 ± 0.5	0.09 ± 0.08	0.03 ± 0.1	0.70 ± 0.7	0.20 ± 0.3
Red blood cells	×10 ⁶ /μL	7.5–9.1	WT	7.9 ± 0.2	8.6 ± 0.6	8.9 ± 0.4	8.6 ± 0.3	9.3 ± 0.2
			<i>Ctsa</i> ^{-/-}	8.1 ± 0.3	8.8 ± 0.4	8.3 ± 0.4	8.3 ± 0.2	7.0 ± 1.4
			scAAV2/8-CTSA	8.2 ± 0.6	8.2 ± 0.5	8.7 ± 0.4	7.8 ± 0.4	8.4 ± 0.5

^aThe range is based on data from mice ages 6–8 weeks provided by St Jude Children's Research Hospitals Veterinary Pathology Core.

CO₂ for 48 h. Following incubation, cells were collected for downstream flow cytometry analyses, and the plate was washed five times with PBS (200 μL/well). The detection antibody was diluted to 1 μg/mL in PBS, containing 0.5% fetal calf serum (PBS-0.5% FCS) and added at 100 μL/well to the plate. The plate was then incubated for 2 h at RT. After washing, the plate was incubated for 1 h at RT with streptavidin-ALP diluted 1:1,000 in PBS-0.5% FCS. Ready-to-use substrate solution (BCIP/NBT-plus) - was added to each well. The plate was developed until distinct spots emerged (about 10 min). Spots were counted using the Molecular Devices Spectramax M5 plate reader.

Flow cytometry analyses

Splenocytes collected at the end of incubation for the ELISpot analyses were transferred to a new 96-well plate. Cells were spun at

1,500 rpm for 5 min at RT, re-suspended, and washed in fluorescence-activated cell sorting (FACS) buffer (10% FBS and 2 mM EDTA in PBS). Cells were then blocked in 100 μL FACS buffer containing anti-CD16/CD32 antibodies, which are directed against Fc receptors, for 10 min at RT. After incubation, 100 μL FACS buffer was added to each well, and the cells were spun at 1,500 rpm for 5 min at RT. Cells were then washed twice in 200 μL FACS buffer and spun at 1,500 rpm for 5 min at RT after each wash. Following the washing steps, cells were incubated in 100 μL FACS buffer containing anti-CD3e-PE, anti-CD4-FITC, anti-CD8-BV605, and anti-CD19-APC for 20 min at RT, in the dark. Following antibody staining, 100 μL FACS buffer was added to each well, and the cells were spun at 1,500 rpm for 5 min at RT. After the last wash, cells were resuspended in FACS buffer containing DAPI and run on a flow cytometer. Data

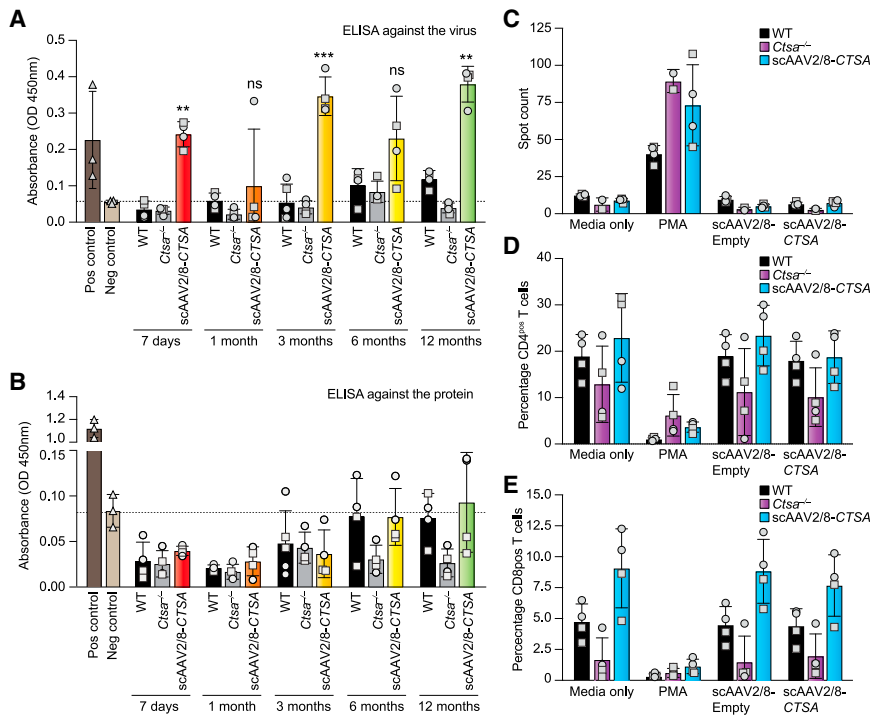


Figure 8. Antibody production and T cell response following treatment with scAAV2/8-CTSA

Levels of neutralizing antibodies against the AAV-2/8 capsid (A) and PPCA transgene product (B) were assessed by ELISA. Anti-PPCA antibody was used as positive control. (C) IFN- γ -specific spot-forming cells were measured via ELISpot for IFN- γ following stimulation of splenocyte samples with scAAV2/8 and scAAV2/8-CTSA. Media from unstimulated splenocytes (medium only) were used as a negative control; PMA-stimulated splenocytes were used as positive control for the assay. Percentage of (D) CD4^{pos} T and (E) CD8^{pos} T cells measured via flow cytometry of cultured splenocyte samples from treated mice following *in vitro* re-exposure to scAAV2/8 capsid and scAAV2/8-CTSA. Data are presented as mean \pm SD. Statistical analyses were performed using the Brown-Forsythe test. ns, not significant; ** $p < 0.01$, *** $p < 0.001$. Round symbols depict males, while square symbols depict females ($n \geq 3$).

collected by flow cytometry were imported into FlowJo software and analyzed for the total percentage of CD4^{pos} and CD8^{pos} T cells.

Statistics

The data are presented as mean \pm SD. Statistical p values of <0.05 were considered significant. Statistical analyses were performed using the Brown-Forsythe test (Figures 2, 3, 8, and S1) with GraphPad Prism, considering that the number of animals was $n < 6$ and that there was an unequal variance among the groups.

Statistics shown in Figure S4 were calculated by the Biostatistics Department at St Jude Children's Research Hospital using pairwise comparisons.

Groups were compared as follows:

Figure 2: To assess the efficacy of the treatment, statistical analyses were performed comparing the treatment groups with the untreated *Ctsa*^{-/-}.

Figure 3: Statistical analyses were performed comparing WT with *Ctsa*^{-/-}, WT with scAAV2/8-CTSA, and *Ctsa*^{-/-} with scAAV2/8-CTSA groups at each time point.

Figure 8A and 8B: Statistical analyses were performed comparing WT with *Ctsa*^{-/-}, WT with scAAV2/8-CTSA, and *Ctsa*^{-/-} with scAAV2/8-CTSA groups at each time point.

Figures 8C–8E: Statistical analyses were performed comparing WT with *Ctsa*^{-/-}, WT with scAAV2/8-CTSA, and *Ctsa*^{-/-} with scAAV2/

8-CTSA groups after re-exposure of the splenocyte cultures to the different agents (medium only, PMA, AAV-empty, and scAAV2/8-CTSA).

Figure S1: To assess the extent of enzyme correction, statistical analyses were performed comparing the treatment groups with WT controls.

Figure S4: The difference in mean vacuolization between WT, *Ctsa*^{-/-}, and scAAV2/8-CTSA groups was examined using linear mixed effects to handle the correlation derived from the repeated measurements ($n = 10$ per mouse) on the same individual mice with a random effect for the mice. Considering there was an overall difference in mean vacuolization, and there was a significant association between vacuolization and the tested groups, we conducted pairwise comparisons among the groups. The results are summarized in two tables shown in the figure.

SUPPLEMENTAL INFORMATION

Supplemental information can be found online at <https://doi.org/10.1016/j.omtm.2021.10.007>.

ACKNOWLEDGMENTS

We thank Richard Ashmun and the staff of the Flow Cytometry and Cell Sorting Shared Resource for their help with FACS analyses and the staff of the Veterinary Pathology Core at St Jude Children's Research Hospital for performing the clinical chemistry and differential blood count analyses, respectively. We are grateful to Aaron Taylor of the Light Microscopy Division of the Cell and Tissue Imaging

Center for his help with the quantification of the correction of tissue morphology and to Mia Panlilio and Khaled Khairy of the Center for Bioinformatics for their support in generating the quantification pipeline. We are indebted to Huiyun Wu and Kumar Srivastava of the Department of Biostatistics for performing statistical tests and biostatistics support. A.d.A. holds the Jewelers for Children Endowed Chair in Genetics and Gene Therapy. This work was funded by NIH grants GM104981 and DK095169, Ultragenyx Pharmaceuticals, the Assisi Foundation of Memphis, and the American Lebanese Syrian Associated Charities (ALSAC).

AUTHOR CONTRIBUTIONS

A.d.A. conceived and designed the study. H.H. coordinated the study and performed immunohistochemistry analyses and the sialic acid content analyses. R.M. performed uptake experiments and enzymatic activities assays. E.G. performed AAV injections and maintained the animal colony. D.v.d.V. assembled the figures and graphical abstract and performed statistical analyses. Y.C. performed the biodistribution analyses. L.E.F. examined the humoral and cellular immune responses. S.A.B. performed the ELISAs against the virus and the transgene. J.A.W. helped with the acquisition and assembly of the immunohistochemistry panels and quantification of tissue morphology. X.Q. purified the anti-PPCA antibody. H.H., I.A., and A.d.A. wrote the manuscript, with input from all the authors. I.A. and A.d.A. reviewed and edited the manuscript. All authors have read and agreed to the published version of the manuscript.

DECLARATION OF INTERESTS

The authors declare no competing interests.

REFERENCES

- Bonten, E.J., Annunziata, I., and d'Azzo, A. (2014). Lysosomal multienzyme complex: pros and cons of working together. *Cell Mol. Life Sci.* *71*, 2017–2032. <https://doi.org/10.1007/s00018-013-1538-3>.
- d'Azzo, A., Andria, G., Bonten, E., and Annunziata, I. (2013). Galactosialidosis, 8th edition. In *The Metabolic and Molecular Bases of Inherited Disease*, C. Scriver, A. Beaudet, W. Sly, and D. Valle, eds. (McGraw-Hill Publishing Co.), pp. 3811–3826.
- Annunziata, I., and d'Azzo, A. (2017). Galactosialidosis: historic aspects and overview of investigated and emerging treatment options. *Expert Opin. Orphan Drugs* *5*, 131–141. <https://doi.org/10.1080/21678707.2016.1266933>.
- d'Azzo, A., Machado, E., and Annunziata, I. (2015). Pathogenesis, emerging therapeutic targets and treatment in sialidosis. *Expert Opin. Orphan Drugs* *3*, 491–504. <https://doi.org/10.1517/21678707.2015.1025746>.
- Zhou, X.Y., Morreau, H., Rottier, R., Davis, D., Bonten, E., Gillemans, N., Wenger, D., Grosveld, F.G., Doherty, P., Suzuki, K., et al. (1995). Mouse model for the lysosomal disorder galactosialidosis and correction of the phenotype with over-expressing erythroid precursor cells. *Genes Dev.* *9*, 2623–2634.
- de Geest, N., Bonten, E., Mann, L., de Sousa-Hitzler, J., Hahn, C., and d'Azzo, A. (2002). Systemic and neurologic abnormalities distinguish the lysosomal disorders sialidosis and galactosialidosis in mice. *Hum. Mol. Genet.* *11*, 1455–1464. <https://doi.org/10.1093/hmg/11.12.1455>.
- Hu, H., Gomero, E., Bonten, E., Gray, J.T., Allay, J., Wu, Y., Wu, J., Calabrese, C., Nienhuis, A., and d'Azzo, A. (2012). Preclinical dose-finding study with a liver-tropic, recombinant AAV-2/8 vector in the mouse model of galactosialidosis. *Mol. Ther.* *20*, 267–274. <https://doi.org/10.1038/mt.2011.227>.
- Leimig, T., Mann, L., Martin Mdel, P., Bonten, E., Persons, D., Knowles, J., Allay, J.A., Cunningham, J., Nienhuis, A.W., Smeyne, R., et al. (2002). Functional amelioration of murine galactosialidosis by genetically modified bone marrow hematopoietic progenitor cells. *Blood* *99*, 3169–3178. <https://doi.org/10.1182/blood.v99.9.3169>.
- Hahn, C.N., del Pilar Martin, M., Zhou, X.Y., Mann, L.W., and d'Azzo, A. (1998). Correction of murine galactosialidosis by bone marrow-derived macrophages over-expressing human protective protein/cathepsin A under control of the colony-stimulating factor-1 receptor promoter. *Proc. Natl. Acad. Sci. U S A* *95*, 14880–14885. <https://doi.org/10.1073/pnas.95.25.14880>.
- Penati, R., Fumagalli, F., Calbi, V., Bernardo, M.E., and Aiuti, A. (2017). Gene therapy for lysosomal storage disorders: recent advances for metachromatic leukodystrophy and mucopolysaccharidosis I. *J. Inher. Metab. Dis.* *40*, 543–554. <https://doi.org/10.1007/s10545-017-0052-4>.
- Rastall, D.P., and Amalfitano, A. (2015). Recent advances in gene therapy for lysosomal storage disorders. *Appl. Clin. Genet.* *8*, 157–169. <https://doi.org/10.2147/TACG.S57682>.
- de Jong, Y.P., and Herzog, R.W. (2021). Liver gene therapy and hepatocellular carcinoma: a complex web. *Mol. Ther.* *29*, 1353–1354. <https://doi.org/10.1016/j.ymthe.2021.03.009>.
- Shirley, J.L., de Jong, Y.P., Terhorst, C., and Herzog, R.W. (2020). Immune responses to viral gene therapy vectors. *Mol. Ther.* *28*, 709–722. <https://doi.org/10.1016/j.ymthe.2020.01.001>.
- Mingozzi, F., and High, K.A. (2013). Immune responses to AAV vectors: overcoming barriers to successful gene therapy. *Blood* *122*, 23–36. <https://doi.org/10.1182/blood-2013-01-306647>.
- Martino, A.T., and Markusic, D.M. (2020). Immune response mechanisms against AAV vectors in animal models. *Mol. Ther. Methods Clin. Dev.* *17*, 198–208. <https://doi.org/10.1016/j.omtm.2019.12.008>.
- Wu, T., Topfer, K., Lin, S.W., Li, H., Bian, A., Zhou, X.Y., High, K.A., and Ertl, H.C. (2012). Self-complementary AAVs induce more potent transgene product-specific immune responses compared to a single-stranded genome. *Mol. Ther.* *20*, 572–579. <https://doi.org/10.1038/mt.2011.280>.
- Yang, F., Patton, K., Kasprzyk, T., Long, B., Gupta, S., Zoog, S.J., Tracy, K., and Vettermann, C. (2021). Validation of an IFN-gamma ELISpot assay to measure cellular immune responses against viral antigens in non-human primates. *Gene Ther.* <https://doi.org/10.1038/s41434-020-00214-w>.
- Colon-Thillet, R., Jerome, K.R., and Stone, D. (2021). Optimization of AAV vectors to target persistent viral reservoirs. *Virology* *18*, 85. <https://doi.org/10.1186/s12985-021-01555-7>.
- Rabinowitz, J.E., Rolling, F., Li, C., Conrath, H., Xiao, W., Xiao, X., and Samulski, R.J. (2002). Cross-packaging of a single adeno-associated virus (AAV) type 2 vector genome into multiple AAV serotypes enables transduction with broad specificity. *J. Virol.* *76*, 791–801. <https://doi.org/10.1128/jvi.76.2.791-801.2002>.
- Kattenhorn, L.M., Tipper, C.H., Stoica, L., Geraghty, D.S., Wright, T.L., Clark, K.R., and Wadsworth, S.C. (2016). Adeno-associated virus gene therapy for liver disease. *Hum. Gene Ther.* *27*, 947–961. <https://doi.org/10.1089/hum.2016.160>.
- Naso, M.F., Tomkowicz, B., Perry, W.L., 3rd, and Strohl, W.R. (2017). Adeno-associated virus (AAV) as a vector for gene therapy. *BioDrugs* *31*, 317–334. <https://doi.org/10.1007/s40259-017-0234-5>.
- Platt, F.M., d'Azzo, A., Davidson, B.L., Neufeld, E.F., and Tiff, C.J. (2018). Lysosomal storage diseases. *Nat. Rev. Dis. Primers* *4*, 27. <https://doi.org/10.1038/s41572-018-0025-4>.
- Nagree, M.S., Scalia, S., McKillop, W.M., and Medin, J.A. (2019). An update on gene therapy for lysosomal storage disorders. *Expert Opin. Biol. Ther.* *19*, 655–670. <https://doi.org/10.1080/14712598.2019.1607837>.
- Riviere, C., Danos, O., and Douar, A.M. (2006). Long-term expression and repeated administration of AAV type 1, 2 and 5 vectors in skeletal muscle of immunocompetent adult mice. *Gene Ther.* *13*, 1300–1308. <https://doi.org/10.1038/sj.gt.3302766>.
- Ferla, R., Alliegro, M., Dell'Anno, M., Nusco, E., Cullen, J.M., Smith, S.N., Wolfsberg, T.G., O'Donnell, P., Wang, P., Nguyen, A.D., et al. (2021). Low incidence of hepatocellular carcinoma in mice and cats treated with systemic adeno-associated viral vectors. *Mol. Ther. Methods Clin. Dev.* *20*, 247–257. <https://doi.org/10.1016/j.omtm.2020.11.015>.

26. Takahashi, H., Hirai, Y., Migita, M., Seino, Y., Fukuda, Y., Sakuraba, H., Kase, R., Kobayashi, T., Hashimoto, Y., and Shimada, T. (2002). Long-term systemic therapy of Fabry disease in a knockout mouse by adeno-associated virus-mediated muscle-directed gene transfer. *Proc. Natl. Acad. Sci. U S A* 99, 13777–13782. <https://doi.org/10.1073/pnas.222221899>.
27. Franco, L.M., Sun, B., Yang, X., Bird, A., Zhang, H., Schneider, A., Brown, T., Young, S.P., Clay, T.M., Amalfitano, A., et al. (2005). Evasion of immune responses to introduced human acid alpha-glucosidase by liver-restricted expression in glycogen storage disease type II. *Mol. Ther.* 12, 876–884. <https://doi.org/10.1016/j.ymthe.2005.04.024>.
28. Murphy, S.L., Li, H., Zhou, S., Schlachterman, A., and High, K.A. (2008). Prolonged susceptibility to antibody-mediated neutralization for adeno-associated vectors targeted to the liver. *Mol. Ther.* 16, 138–145. <https://doi.org/10.1038/sj.mt.6300334>.
29. Cresawn, K.O., Fraites, T.J., Wasserfall, C., Atkinson, M., Lewis, M., Porvasnik, S., Liu, C., Mah, C., and Byrne, B.J. (2005). Impact of humoral immune response on distribution and efficacy of recombinant adeno-associated virus-derived acid alpha-glucosidase in a model of glycogen storage disease type II. *Hum. Gene Ther.* 16, 68–80. <https://doi.org/10.1089/hum.2005.16.68>.
30. Nienhuis, A.W., Nathwani, A.C., and Davidoff, A.M. (2016). Gene therapy for hemophilia. *Hum. Gene Ther.* 27, 305–308. <https://doi.org/10.1089/hum.2016.018>.
31. Nathwani, A.C., Reiss, U.M., Tuddenham, E.G., Rosales, C., Chowdhary, P., McIntosh, J., Della Peruta, M., Lheriteau, E., Patel, N., Raj, D., et al. (2014). Long-term safety and efficacy of factor IX gene therapy in hemophilia B. *N. Engl. J. Med.* 371, 1994–2004. <https://doi.org/10.1056/NEJMoa1407309>.
32. Hinderer, C., Katz, N., Buza, E.L., Dyer, C., Goode, T., Bell, P., Richman, L.K., and Wilson, J.M. (2018). Severe toxicity in nonhuman primates and piglets following high-dose intravenous administration of an adeno-associated virus vector expressing human SMN. *Hum. Gene Ther.* 29, 285–298. <https://doi.org/10.1089/hum.2018.015>.
33. Flotte, T.R., and Buning, H. (2018). Severe toxicity in nonhuman primates and piglets with systemic high-dose administration of adeno-associated virus serotype 9-like vectors: Putting patients first. *Hum. Gene Ther.* 29, 283–284. <https://doi.org/10.1089/hum.2018.021>.
34. Han, Z., Zhong, L., Maina, N., Hu, Z., Li, X., Chouthai, N.S., Bischof, D., Weigel-Van Aken, K.A., Slayton, W.B., Yoder, M.C., et al. (2008). Stable integration of recombinant adeno-associated virus vector genomes after transduction of murine hematopoietic stem cells. *Hum. Gene Ther.* 19, 267–278. <https://doi.org/10.1089/hum.2007.161>.
35. Inagaki, K., Piao, C., Kotchey, N.M., Wu, X., and Nakai, H. (2008). Frequency and spectrum of genomic integration of recombinant adeno-associated virus serotype 8 vector in neonatal mouse liver. *J. Virol.* 82, 9513–9524. <https://doi.org/10.1128/JVI.01001-08>.
36. Smith, R.H. (2008). Adeno-associated virus integration: virus versus vector. *Gene Ther.* 15, 817–822. <https://doi.org/10.1038/gt.2008.55>.
37. Deyle, D.R., and Russell, D.W. (2009). Adeno-associated virus vector integration. *Curr. Opin. Mol. Ther.* 11, 442–447.
38. Colella, P., Ronzitti, G., and Mingozi, F. (2018). Emerging issues in AAV-mediated in vivo gene therapy. *Mol. Ther. Methods Clin. Dev.* 8, 87–104. <https://doi.org/10.1016/j.omtm.2017.11.007>.
39. Nguyen, G.N., Everett, J.K., Kafle, S., Roche, A.M., Raymond, H.E., Leiby, J., Wood, C., Assenmacher, C.A., Merricks, E.P., Long, C.T., et al. (2021). A long-term study of AAV gene therapy in dogs with hemophilia A identifies clonal expansions of transduced liver cells. *Nat. Biotechnol.* 39, 47–55. <https://doi.org/10.1038/s41587-020-0741-7>.
40. Li, Y., Miller, C.A., Shea, L.K., Jiang, X., Guzman, M.A., Chandler, R.J., Ramakrishnan, S.M., Smith, S.N., Venditti, C.P., Vogler, C.A., et al. (2021). Enhanced efficacy and increased long-term toxicity of CNS-directed, AAV-based combination therapy for Krabbe disease. *Mol. Ther.* 29, 691–701. <https://doi.org/10.1016/j.ymthe.2020.12.031>.
41. Dalwadi, D.A., Torrens, L., Abril-Fornaguera, J., Pinyol, R., Willoughby, C., Posey, J., Llovet, J.M., Lanciault, C., Russell, D.W., Grompe, M., et al. (2021). Liver injury increases the incidence of HCC following AAV gene therapy in mice. *Mol. Ther.* 29, 680–690. <https://doi.org/10.1016/j.ymthe.2020.10.018>.
42. Arruda, V.R., and Doshi, B.S. (2020). Gene therapy for hemophilia: Facts and Quandaries in the 21st century. *Mediterr. J. Hematol. Infect Dis.* 12, e2020069. <https://doi.org/10.4084/MJHID.2020.069>.
43. Russell, W.M.S., and Burch, R.L. (1959). *The Principles of Humane Experimental Technique*.
44. Allay, J.A., Sleep, S., Long, S., Tillman, D.M., Clark, R., Carney, G., Fagone, P., McIntosh, J.H., Nienhuis, A.W., Davidoff, A.M., et al. (2011). Good manufacturing practice production of self-complementary serotype 8 adeno-associated viral vector for a hemophilia B clinical trial. *Hum. Gene Ther.* 22, 595–604. <https://doi.org/10.1089/hum.2010.202>.